Water Oscillation Modelling Inside the Oscillating Water Column for Wave Energy Conversion

Abdelhamid El Barakaz‡, Abdellatif El Marjani

EMISys Research Team, Engineering 3S Research Center, Turbomachinery Lab. Mohammadia School of Engineers,

Mohammed V University in Rabat

B.P. 765 Agdal, Rabat, Morocco

E-mail: elbarakaz.abdelhamid@gmail.com, elmarjani@emi.ac.ma

‡ Corresponding Author: Abdelhamid El Barakaz, B.P. 765 Agdal, Rabat, Morocco; tel: +212 613 098 159

elbarakaz.abdelhamid@gmail.com

Abstract– Among wave energy converters (WECs), the Oscillating Water Column (OWC) system is considered as one of the most promising converters; this system works on the principle of water oscillations in an enclosed air chamber due to incident sea waves. The amount of the harvested pneumatic power depends on the elevation level, the water oscillations' frequency inside the chamber, and the chamber's global damping. A one-dimensional (1-D) unsteady model has been elaborated to analyze the water elevation's dynamic behaviour. Great attention has been paid to determine the natural frequency and the global damping for maximum wave energy capture. The model is based on a water mass block moving periodically upward and downward as a piston inside the chamber, inducing the enclosed air to flow alternately through a turbine. The Lagrangian formalism has been adopted to derive the governing differential equation for the piston water motion. Then the poincaré-Lindstedt method has been used to deal with the non-linearity of the problem. The elaborated model has been adapted to an OWC system in the case of monochromatic waves. Results have been compared to another referenced paper for validation and pertinence, fair agreements have been noted.

Nomenclature:

A	Chamber length
B	Chamber width
C	Turbine damping coefficient
d	Chamber submerged length
D_{epth}	Chamber sea depth
F	External force
g	Local gravity acceleration
$\widetilde{H}$	Elevation of sea waves
$\widetilde{H}_{max}$	Sea waves maximum elevation
H	Piston elevation
H_{max}	Piston maximum elevation
h	Water elevation inside the chamber
h_{max}	Water maximum elevation inside the chamber
$\dot{h}$	Water velocity inside the chamber

$\ddot{h}$	Water acceleration inside the chamber
L	Height of the chamber
L^*	Lagrangian
M	Mass of water inside the chamber
P	Air pressure inside the chamber
P_0	Atmospheric pressure
Q	Airflow rate
S	Chamber base area
T	Wave period
T^*	Kinetic energy
V^*	Potential energy
x_i	Poincaré-Lindstedt functions
v	Wave velocity
γ	OWC global damping coefficient
ϵ, φ	Parameters of the Poincaré–Lindstedt method
λ	Wavelength
μ	Energy loss coefficient
ρ_e	Seawater density
Ω	Incoming waves frequency
ω_0	Natural fundamental frequency
ω_1	Natural first frequency

1. Introduction

Nowadays, renewable energy has gained significant interest due to the growing concerns about the climate change challenge. Some countries made massive efforts for more renewable energy integration, particularly for solar and wind energy:

On the one hand, solar power may be the hope of tomorrow's energy revolution; sunlight that reaches the earth's surface is the most abundant energy resources on our planet. One hour of received solar power can satisfy the human requirement of an entire year. It can be exploited directly using photovoltaics (PV): Monocrystalline, polycrystalline and microcrystalline silicon are commonly used as semiconductors in photovoltaic systems. [1] [2], there is also oriented research projects to the dye-sensitized solar cells (DSSCs), which have encouraging results for next-generation solar cells due to their relatively low cost and good efficiency [3] [4] [5]. Sunlight can also be exploited indirectly using concentrated solar power (CSP). In this case, plants engage collectors (aligned mirrors or lenses) to converge sunlight from a wide surface into a small one; increasing the light's intensity helps produce high temperatures between 800°C and 2,000 °C. This heat operates a boiler, which in turn generates

steam for a steam turbine. many industrialized countries are investing in CSP technology because of its capacity for bulk electricity generation. [6]

On the other hand, Wind energy has always been convenient, efficient for daily needs; it is usually harvested using wind turbines; each turbine has a unique technical identity in terms of the used design. Since 1980, advances in aerodynamics and structural dynamics contributed to a 5% annual increase in the energy efficiency of wind turbines. Today we find some installed wind turbine that can reach up to 3 MW due to their advanced design and massive wind kinetic energy capture capacity. Offshore has better potential since wind speed at sea is 70 to 100% higher and much more constant. [7] [8]

Besides solar and wind energy, ocean energy has started to gain interest since the 70s. This energy is a high-quality source of renewable energy that presents enormous potential for exploitation. This energy category includes ocean tidal energy, wave energy, energy from marine currents, thermal gradient, and salinity gradient. Various solutions have been considered to exploit this kind of energy, such as power buoy, wave dragon, oscillating water column (OWC), Pelamis, reversed electrodialysis (RED), pressure-retarded osmosis (PRO) …[9] [10] [11] [12].

Wave energy, which derives from solar energy and presents a form of high-density energy storage, is a relatively perpetual and highly predictable category of energy. Indeed, solar power density average on earth is about $100W/m^2$, which can be eventually transformed into a wave power concentration of over 60kW/m [13]; this represents a significant potential for wave energy harvesting, especially in some world regions, as shown indicatively in Figure 1.

Figure 1: World wave power estimation in kW/m

Ocean waves are formed due to the imbalance between gravitational and wind shear forces. As waves travel from deep to shallower water, a certain amount of energy dissipates. Nevertheless, wave power available in the nearshore is enough to produce electrical energy, and it depends on wave amplitude and frequency [14]. Extracting energy from waves has been extensively followed over the last few decades. One of the most studied devices for extracting sea waves energy is the oscillating water column (OWC). This system consists essentially of two elements: a chamber which is generally made of concrete, and a turbine generator group that converts

wave energy into electricity. This system has two major benefits, the first one is its simplicity, and the second one concerns the maintenance costs, which are lower than other WECs since the Power Take-Off (PTO) system is not in direct contact with seawater.

As shown in Figure 2, any OWC system consists of a submerged air chamber in the sea connected to the atmosphere through a circular duct where an air turbine is installed. The oscillatory water movement inside the chamber generates inhalation and exhalation, which induces a bidirectional flow through the turbine. Despite airflow direction changes, the turbine's rotational movement should be in the same direction. Turbines like Wells, radial, or axial impulse and other types match these specific conditions [15] [16]. This process is responsible for converting the chamber pneumatic energy into a mechanical one then into electricity via a generator, providing the necessary power for daily uses.
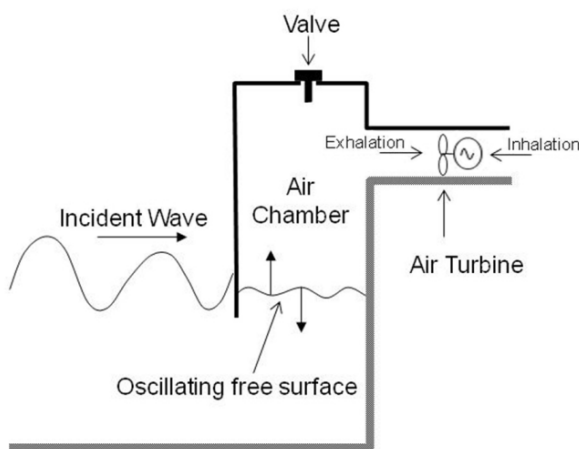
Figure 2: OWC working principle

The OWC concept idea is not new. In 1910, the French Bochaux-Praceique started developing one of the first applications using wave energy for electricity home supply at Royan (France) and used a pneumatic system to create the first oscillating water column [17], as shown in Figure 3 below.
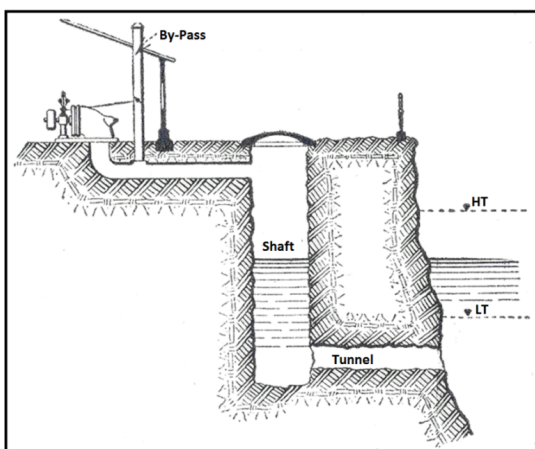
Figure 3: Illustration of Bochaux-Praceique OWC device from the magazine Power [17]

In 1947, Yoshio Masuda, a Japanese naval commander, designed an OWC navigation buoy that used a turbine system to generate electricity, recharge the buoy's batteries continuously, and give some autonomy engine [18]. Since the 1980s, several types of OWC devices have been developed, built, and tested for offshore floating and onshore OWCs; they are successful operating devices, especially in some locations, as shown in Table 1.

Table 1: Examples of typical OWC plants in the world.

	Location	Power
PICO	Azores	400 kW
LIMPET	Islay Island	500 kW
OSPREY	Scotland	2 MW
SAKATA	Japan	60 kW

The amount of energy, which could be converted into a useful form, depends strongly on the chamber's flow behaviour and the turbine used for pneumatic energy conversion. The design of the chamber is also a key for high performances. Indeed, analyses always aim to find regimes of high amplification of waves inside the chamber for maximum energy generation. However, to improve the energetic global performances, the viscous flow's aerodynamic losses should be controlled [19]. Also, the OWC system must resist challenging environmental conditions with high waves loads under storm conditions.

Several studies of mathematical and numerical analysis of the OWC hydrodynamics have been established, including 2D and 3D models. Objectives refer to deal with the hydrodynamic and the aerodynamic coupling inside the chamber [20] [21] [22] [23] [24] [25], besides the improvement of the turbine performances [26] [27]; in this context, attempts aimed to describe the dynamics of water surface behaviour inside the chamber. The purpose is to maximize the power recuperation from waves by exploiting the resonance phenomenon depending on the global damping and the natural frequency of the OWC system. In order to achieve this objective, a simple one-dimensional piston model has been elaborated in the present work to investigate the water elevation dynamic behaviour and its impact on the OWC global performances.

2. Modelling and Lagrangian Formalism:

2.1. Modelling Description and Assumptions:

All general assumptions made in the modelling approach are described as follows:
> The chamber free water surface is assumed to behave as a piston able to move only in the vertical direction.
> The air density variation inside the chamber is neglected; the air is considered incompressible because of its low velocity in the operating conditions (Mach number < 0.3) [28].

➢ The hydraulic energy losses via the viscosity of fluids and frictions are neglected.

➢ The pneumatic energy losses in the duct and the air turbine are neglected.

➢ The incoming sea waves are monochromatic. Reflected, diffracting, and radiation flows are not considered for the studied piston model.

➢ The pressure inside the chamber depends only on turbine characteristics (turbine equation).

➢ The origin of wave elevation (*H=0*) coincides with the equilibrium sea level.

➢ *Z*-axis is pointing upward in the vertical direction.

➢ The cross-section *S* of the chamber is constant.

➢ The OWC system is operating in deep water (*h<< D_epth*).

In this study, it is considered that the water surface inside the chamber oscillates with an amplitude h_{max} and a frequency ω under the influence of the incoming waves characterized by their amplitude H_{max} and frequency Ω. The chamber has zero thickness, area *S*, height *L*, width *B*, length *d* for the submerged portion, and a water depth D_{epth} under the chamber. Air pressure inside and outside the chamber are respectively *P* and *P₀* (atmospheric pressure). A pressure difference *ΔP=P-P₀* occurs only in the duct where a Wells turbine is installed. These operating parameters and conditions are depicted in Figure 4.
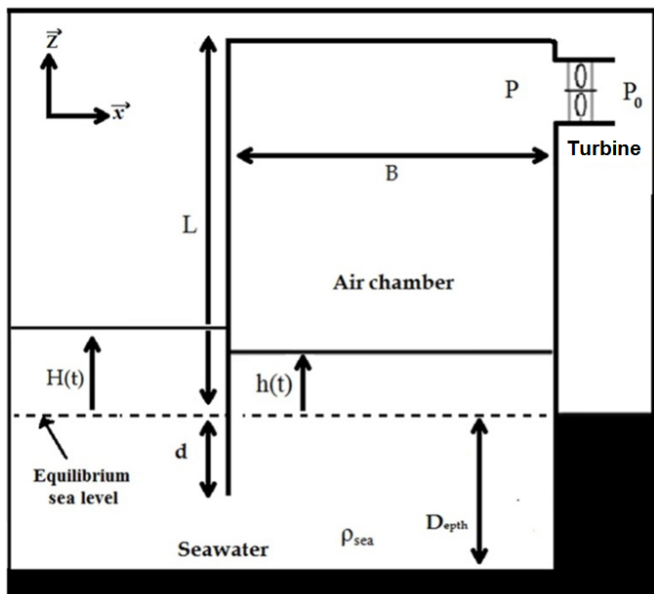
Figure 4: Geometry and characteristics of the chamber

2.2. The Piston Model:

Sea waves are described by their temporal-spatial variations; each point of the sea surface is defined by its coordinates *(x,y)* and has its elevation *h* in an instant t $h \rightarrow f_{\vec{z}}(x, y, t)$. The objective of this part is to simplify the study

and find an equivalent model with the same effect on the chamber aerodynamics that generates the same airflow; this can be done by adopting the piston model in which all points of water surface elevation inside the chamber have the same value h(t).

The simplest mathematical way to describe ocean wave propagation is Airy's theory, which is often called the linear wave theory. This theory is based on the assumptions formulated by Airy (1845) and describes the propagation of waves in the sea. One of the basics of Airy's assumptions is the existence of velocity potential that satisfies Laplace's equation in deep water (*h<< D_epth*) [29]

According to this theory, the surface elevation of waves is described by a sinusoidal curve; it is a function of the horizontal position *x* and time *t*. Due to the symmetry of the incident wave, it is invariant in the y-direction. The surface elevation $\widetilde{H}(x, t)$ depicted in Figure 5 is expressed as follows:

$$\widetilde{H}(x,t) = \widetilde{H}_{max} sin\ (2\pi(x - vt)/\lambda) \qquad (1)$$

Or:

$$\widetilde{H}(x,t) = \widetilde{H}_{max} sin\ (2\pi x/\lambda - 2\pi t/T) \qquad (2)$$
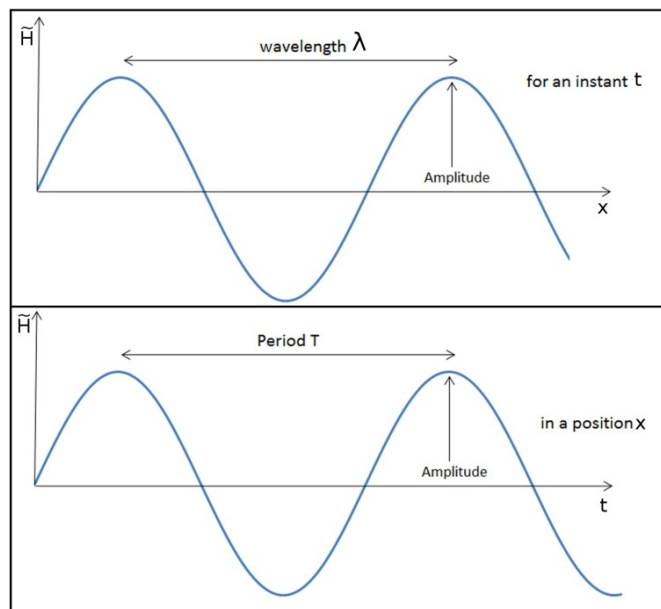
Figure 5: Illustration of the time-space variation of sea waves

The following equation associates λ and T and usually called the "dispersion equation" [30] [25]:

$$(2\pi/T)^2 = (2\pi g/\lambda)tanh\ (2\pi D_{epth}/\lambda) \qquad (3)$$

Water oscillations inside the chamber, in the present model, are presented with a mass block acting as a piston for which the vertical elevation *H(t)* has been assigned at the averaged wave elevation of $\widetilde{H}(t, x)$ over chamber width *B*, the average method aims to eliminate the spacial variation of the wave in the $\vec{x}$ direction and come up with a wave function with the same effect on the airflow inside the chamber, as shown in Figure 6. In this part, the geometrical effect has been

considered to determine the wave's average inside the chamber.
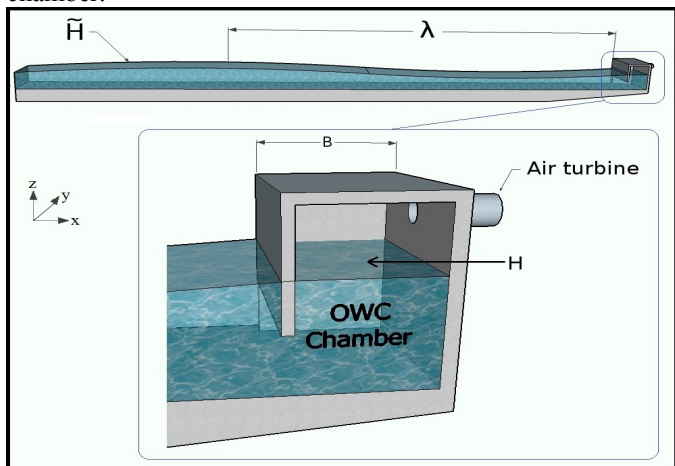
Figure 6: Water piston modelling

The vertical piston elevation $H(t)$ is given by:

$$H(t) = \frac{1}{B}\int_0^B \widetilde{H}(t,x)dx \qquad (4)$$

Hence:

$$H(t) = \widetilde{H}_{max}\frac{sin(\pi B/\lambda)}{\pi B/\lambda}sin(\pi B/\lambda - 2\pi t/T)$$
$$= H_{max}\,sin(\pi B/\lambda - 2\pi t/T) \qquad (5)$$

Where:

$$H_{max} = \widetilde{H}_{max}\frac{sin(\pi B/\lambda)}{\pi B/\lambda} \qquad (6)$$

It can be perceived from equation (6) that the amplitude of the piston oscillations H_{max} depends on the wavelength λ and the chamber width B. The variation of these parameters is represented in the graph of Figure 7.
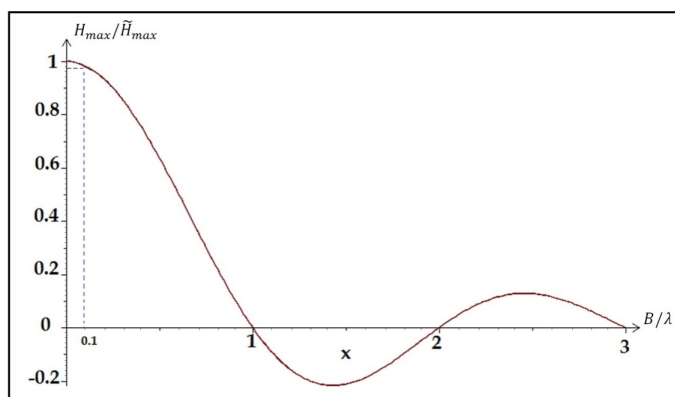
Figure 7: Piston to wave amplitude ratio variation with B/λ

In the graph depicted in Figure 7, if the width B is a multiplier of λ waves the piston elevation is nullified even with the presence of incident waves: waves do not generate any airflow inside the chamber. However, it can be observed that in the region where the ratio B/λ is low, this effect can be neglected. In fact, in the operating conditions, wavelength determined from the dispersion relation in equation (3) is usually higher than 100m; the typical width B is generally

taken around 10m in most OWC realizations [31]. Hence, the ratio B/λ is practically about 1/10, which corresponds according to Figure 7 to a ratio $H_{max}/\widetilde{H}_{max}$ of 97%.

One of the factors to design the OWC chamber is the wavelength of incoming waves, which depends on sea depth. This is one reason to explain why larger scale OWCs are deployed in deep water, unlike small OWCs projects deployed in shallow water [32].

2.3. Lagrange Method:

The OWC system is physically studied by considering a vertical oscillating water piston as a block of water mass M under the influence of upper air pressure force F_1, the lower water pressure force F_2, and the water piston own weight, as shown in Figure 8.
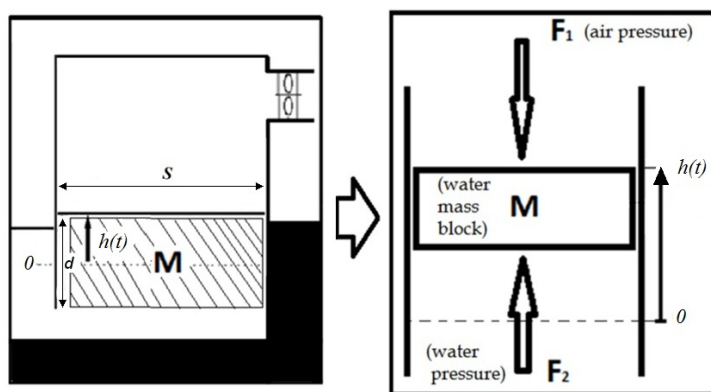
Figure 8: Oscillating water piston model

The expression of piston mass M is related to water elevation inside the chamber as given in equation (7):

$$M(t) = \rho_e\, S\, (h(t) + d) \qquad (7)$$

The expression of F_1 depends on the turbine type. Wells or impulse turbines are the most popular in practical applications [33]. The relation between the pressure drop ΔP and the flow rate Q inside an air turbine is described as $\Delta P = CQ^n$ [34] where C is the damping coefficient related to the used turbine and n is equal to 1 and 2 in Wells and impulse turbine, respectively.

In our case, a linear relation of Wells turbine was considered to simplify the mathematical resolution, where the damping equation can be expressed as:

$$\Delta P = CQ \qquad (8)$$

Both fluids, water and air, are incompressible in the OWC conditions. The flow rate inside the chamber is expressed as follows:

$$Q = S\,\dot{h} \qquad (9)$$

F_1 is related directly to the applied air pressure:

$$F_1 = S\,P_0 + C\,S^2\,\dot{h} \qquad (10)$$

The applied force by water pressure F_2 depends on sea level:

$$F_2 = S\,(P_0 + g\,\rho_e(H(t) + d)) \qquad (11)$$

The previous expressions of M, F_1 and F_2 has been used in Lagrange formulation in the mathematical model to establish

the differential equation governing the piston motion as detailed in Appendix A [35].

Finally, the differential equation of water elevation inside the chamber can be expressed as follows [36] [37] [38]:

$$\underbrace{\ddot{h} + \gamma\,\dot{h} + \omega_0^2\,h}_{linear} + \underbrace{\frac{1}{d}\left[h\,\ddot{h} + \frac{1}{2}\dot{h}^2\right]}_{non\ linear} = \frac{g}{d}H(t)$$

(12)

$$\text{With}: \begin{cases} \omega_0 = \sqrt{g/d} \\ \gamma = {C\,S}/{\rho_e\,d} \end{cases}$$

The differential equation (12) can be otherwise demonstrated with a second method by considering the Euler equation inside a U tube with conditions similar to the OWC chamber oscillations (see Appendix B).

At first glance, this differential equation can be separated into a linear part, similar to a second-order oscillator responsible for wave oscillations inside the chamber, and a nonlinear part that perturbs the motion regularity of waves.

3. Poincaré–Lindstedt Method:

The previous differential equation (12) is analytically solved using Henri Poincaré and Anders Lindstedt's method; it is based on removing unbounded secular terms, especially in weakly nonlinear problems [39]. This method is generally used to approximate the periodic solutions of ordinary differential equations with nonlinear terms.

In our study, two cases have been analyzed for the homogeneous and non-homogeneous equations.

3.1. The Homogeneous Differential Equation $H(t) = 0$:

In this section, equation (12) is considered without the exciter term. The OWC system is perturbed by raising the water level inside the chamber h to maximum level h_{max}. As a consequence, it will oscillate according to the natural frequency of the OWC device. This description corresponds to the following initial conditions:

$$\begin{cases} h(0) = h_{max} \\ \dot{h}(0) = 0 \end{cases}$$

(13)

3.1.1. Case 1: The Harmonic Oscillations ($\gamma = 0$)

After calculation detailed in Appendix C using Poincaré–Lindstedt method, the solution $h(t)$ can be written as:

$$h(t) = h_{max}\,cos(\omega_0 t) + h_{max}^2(1 - cos^2(\omega_0 t))/2d \quad (14)$$

The solution of the differential equation has been plotted in Figure 9. It is almost a sinusoidal motion. The analytical solution $h(t)$ is the sum of the linear solution term $x_0(\varphi)$ and the additionnal nonlinear term $\epsilon x_1(\varphi)$ (see Appendix C) It can be observed that the motion is nearly similar to the movement of a classical second-order oscillator system.
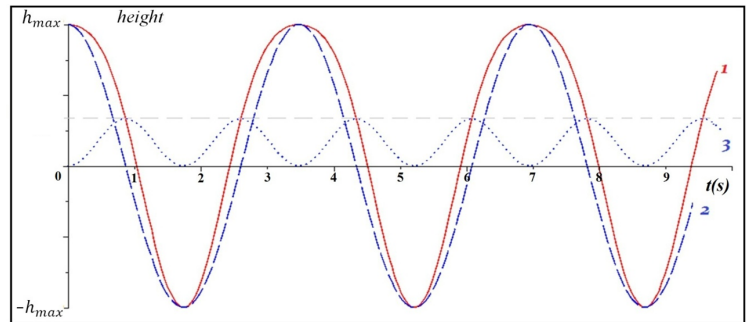
Figure 9: Piston motion: (1) Poincaré–Lindstedt solution h(t), (2) linear solution $x_0(\varphi)$, (3) nonlinear solution $\epsilon x_1(\varphi)$

As shown in the previous graph, the nonlinear term affects only the shape of $h(t)$ graph concerning the time-axis [40], while the natural frequency remains the same. However, in the case of low wave elevation comparing to the submerged length d, the coefficient ϵ would be very small, so the linear curve is approximately matching the Poincaré–Lindstedt solution. In this case, the linear model is a sufficient approximation for the water piston motion.

By applying the same method and using an analogy with the calculation presented in Appendix C, we can conclude the results for the other cases: under-damping, over-damping, and critical damping case [41].

3.1.2. Case 2: The Under-damping: ($\gamma < 2\omega_0^2$)

For the under-damped system, it can be noticed that the solution is a sinusoidal motion that slowly decreases in magnitude until it equals zero (Figure 10). After the first two periods, the damping phenomenon dominates the non-linearity effect.
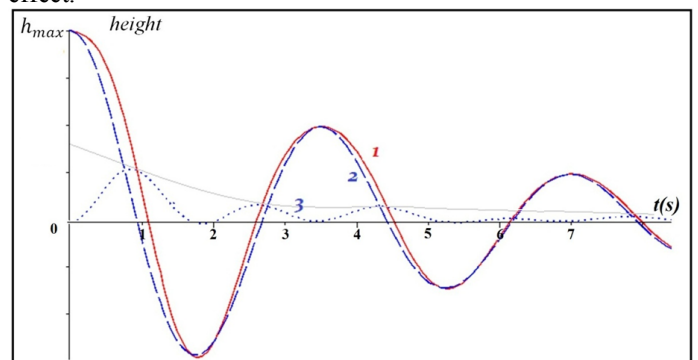
Figure 10: Under-damping case: (1) Poincaré–Lindstedt solution $h(t)$, (2) linear solution $x_0(\varphi)$, (3) nonlinear solution $\epsilon x_1(\varphi)$

3.1.3. Case 3: The Over-damping and Critical damping:($\gamma \geq 2\omega_0^2$)

For the over-damped $(\gamma > 2\omega_0^2)$ and Critical damped systems $(\gamma = 2\omega_0^2)$, as shown in Figure 11, we notice the absence of oscillations; the solution is an exponential decay over time. Due to the high value of the damping, the non-linearity is dominated by the damping phenomenon. The critically damped motion has the same shape as the over-

damped one but has the property to converge to the origin rapidly.
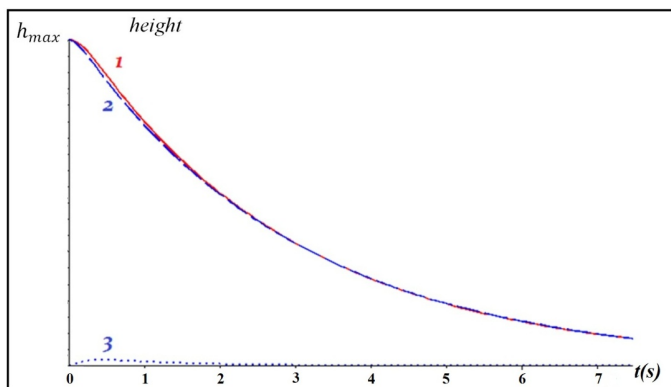
Figure 11: Overdamping and the critical damping case: (1) Poincaré–Lindstedt solution h(t), (2) linear solution $x_0(\varphi)$, (3) nonlinear solution $\epsilon x_1(\varphi)$

3.1.4. The Non-homogenous Differential Equation $H(t) = H_{max}cos(\Omega t) \neq 0$:

In this section, the differential equation (12) is considered with a sinusoidal term on the right-hand side, which expresses the motion of the incoming wave $H(t) = Hcos(\Omega t)$ [42]. Hence, in this case, the piston elevation motion inside the chamber is driven by the incident sea waves.

$$\ddot{h} + \gamma\dot{h} + \omega_0{}^2 h + \epsilon\left[h\ddot{h} + \frac{1}{2}\dot{h}^2\right] \quad (15)$$
$$= (g/d)\mathrm{H}_{max}cos(\Omega t)$$

To realize a study with realistic parameters, we have considered the following chamber dimensions in Figure 12 operating with Wells turbine:
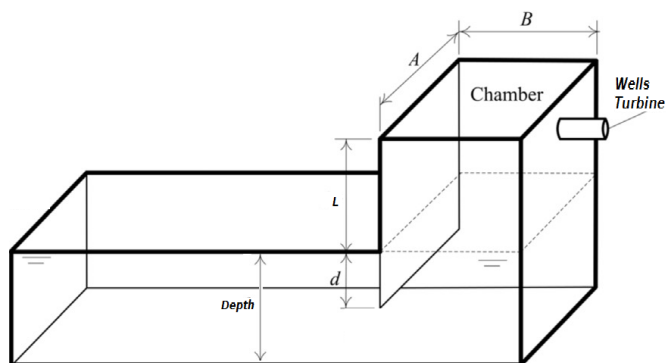
Figure 12: OWC geometry used in reference [43]

In general, variables taken into account for such an energy converter are the geometry, the flow rate, the pressure drop, the rotational speed, the diameter of the turbine, and the fluid density, which has been regarded in assumptions as a constant for simplification. The resulting pneumatic power can be calculated by multiplying the flow rate and the pressure drop. In this section, the incident wave has a period of 9s and an elevation amplitude of 1m, water depth near and under the chamber is equal to 10m, the relation of dispersion presented in Equation (3) gives a wavelength of about 81m, which

means an equivalent piston elevation amplitude of 0,96m. The airflow inside the chamber is imposed by the free water surface, taking into account the rotational speed of Wells turbine approximately 100rad/s with a diameter of 1.5m, which corresponds to a turbine damping coefficient 117.1Pa.m^{-3}.s. [43]. Additional Parameters are in Table 2:

Table 2: Simulation parameters

g = 9.81m/s² ρ_e = 1000 Kg/m³ $H(t) = H_{max}.cos(\Omega t)$ H_{max} =0.96 m Ω= 0.7 rad/s (period of 9 sec) D_{epth}=10m	A=10m B=10m S=100m² d = 2.5 m C = 117.1 Pa.s/m³

Those parameters are the same used by F. R. Torres et al. [43]. Indeed, they developed a numerical analysis of the OWC using the Fluinco model based on a slightly compressible flow method to solve the Navier–Stokes equations. A comparison has been established to reveal the pertinence of the final results. The numerical values of the global damping and the natural frequency of the OWC system are given based on Equation (12) as follows:

$$\begin{cases} \gamma = 4.68 \ s^{-1} \\ \omega_0 = 1.98 \text{rad/s} \end{cases} \quad (16)$$

3.2. Poincaré–Lindstedt First Order Method:

After tremendous and heavy calculations, the Poincaré–Lindstedt first-order method has been applied by limiting the solution decomposition to the usual terms x_0 and x_1, as mentioned in Appendix C. The resulting solutions are depicted in Figure 13.
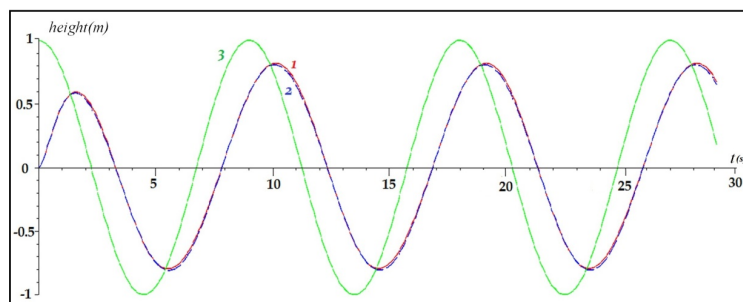
Figure 13: analytical solutions: (1) Poincaré–Lindstedt solution $h(t)$, (2) the linear solution $x_0(\varphi)$, (3) the incident wave motion $H(t)$)

The analytical and linear solutions shown respectively by curves 1 and 2 in Figure 13 are almost identical. The non-linearity has no significant effect on the appearance of the graph solution. This fact remains valid as long as the incoming waves' magnitude is small compared to the length of the submerged portion of the chamber d (see Appendix C calculation). In this case, the ratio H_{max}/d is equal to 38.4% and we found a good matching between the first-order Poincaré–Lindstedt solution and the linear solution.

3.3. Simulink

A state-space description is needed to simulate OWC behaviour in Simulink software with Table 2 parameters. It is a mathematical representation of the OWC system with inputs, outputs, and state variables related to each other by first-order differentiation. Equation (15) can be written as a system of three equations to build the state-space model with $H(t)$ as the input and $h(t)$ as the output. The system (17) can be illustrated through the state-space model in Figure 14.

$$\begin{cases} \ddot{h} = \left(g/d\right)Hcos(\Omega t) - \gamma \dot{h} - \omega_0^2 h - \epsilon\left[h\ddot{h} + 1/2\,\dot{h}^2\right] \\ \dot{h} = \int \ddot{h} \\ h = \int \dot{h} \end{cases} \quad (17)$$
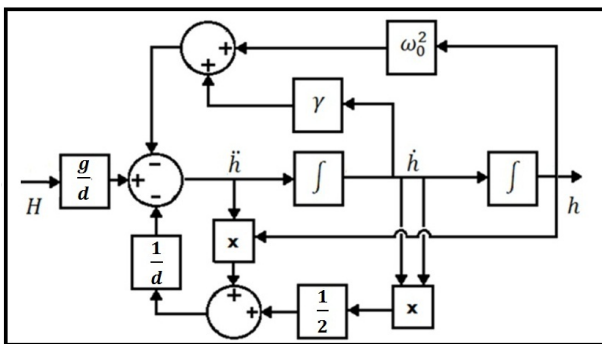
Figure 14: State-space model of the OWC

The state-space model has been rebuilt in Simulink with input signal $Hcos(\Omega t)$ and output h, both are plotted through a scope block attached, as shown in Figure 15.
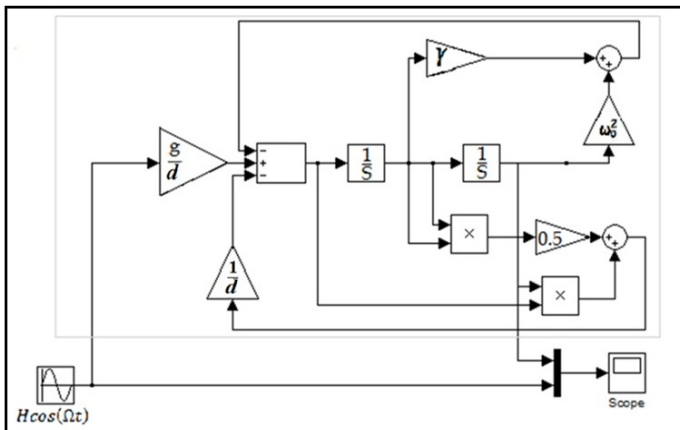
Figure 15: State-space of the OWC on Simulink software

The comparison of the obtained solution, respectively, with Simulink software Figure 16–a, and Poincaré–Lindstedt method Figure 16-b, shows that solutions are very similar. The adopted solving methods are compatible with each other.
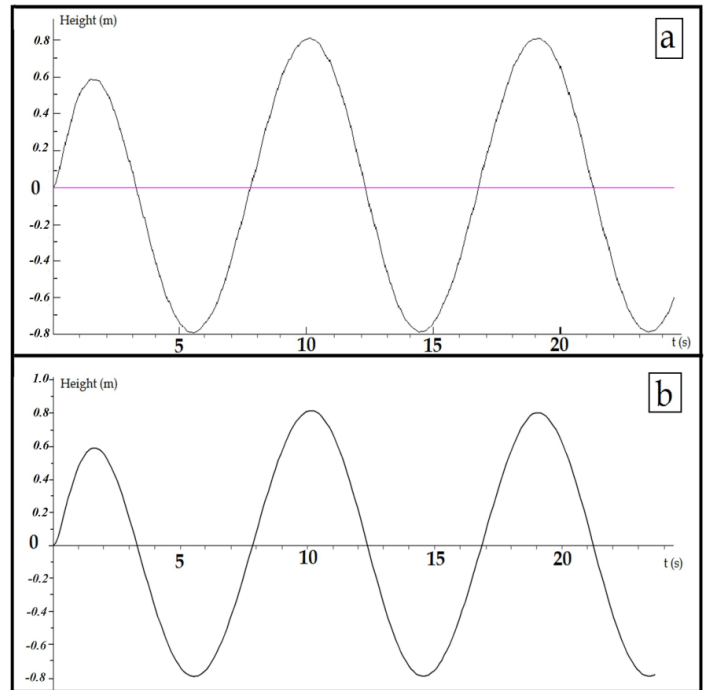
Figure 16: Solutions comparison: Simulink software (a), Poincaré–Lindstedt method (b)

In Figure 17, an FFT analysis (Fast Fourier Transform) has been established for Simulink's result to determine the effect of the non-linearity of the differential equation terms, particularly on the solution modes: the fundamental mode is the most dominant one, other modes are missing in this case.
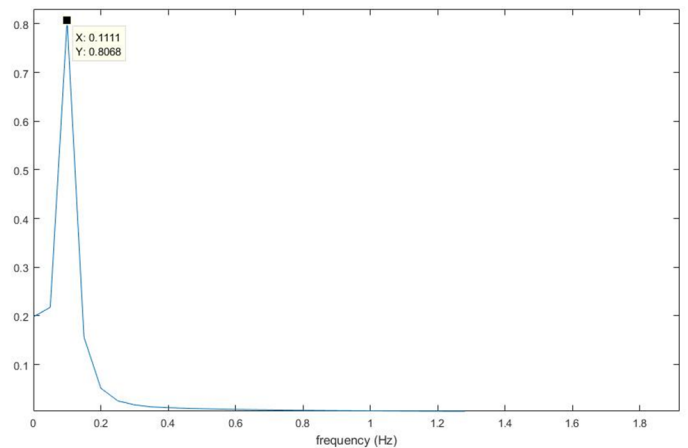
Figure 17: Positive FFT of the analytical solution h(t)

3.4. Results Validation:

The obtained previous results are now compared to those of F. R. Torres model results and plotted in the same interval (125s to 180s), as shown in Figure 18.
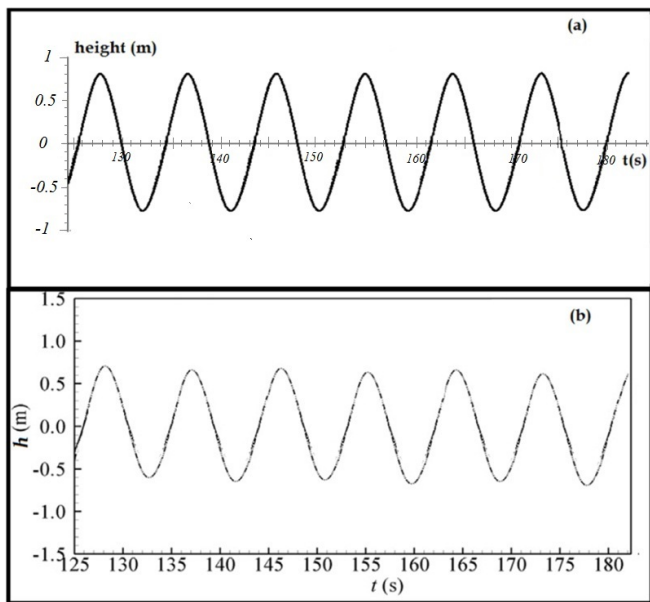
Figure 18: Comparison of solutions: Poincaré–Lindstedt method (a), F. R. Torres et al. (b)

Figure 19: Analytical pressure drop through the turbine (a) Pressure drop in the turbine by F. R. Torres et al. (b)

Results obtained with the Poincaré–Lindstedt first-order method and F. R. Torres simulation are very similar. The highest level h_{max} reached by water in Poincaré–Lindstedt method is 0.78m. In F.R. Torres reference used for comparison h_{max} is equal to 0.75m. It can be observed that both graphs show insignificant differences taking into account that the respective solutions are obtained from two different resolution methods for the same OWC parameters and dimensions.

Another comparison can be established by calculating the duct pressure drop. In our case, we used the Wells turbine linear law:

$$\Delta P = CQ = CS\dot{h} \qquad (18)$$

The pressure drop graphs are shown in Figure 19-a and Figure 19-b for both models and for the same time-domain (125s -180s):

The graphs obtained are almost the same. The maximum variation ΔP_{max} is equal to 3.5 kPa in the present model versus the estimated value of 3.8kPa in the model developed by F. R. Torres et al. It can be observed that the pressure variations are minor. Hence, air density inside the chamber may be considered constant during inhalation and exhalation, which confirms the assumption that air is an incompressible fluid in the operating conditions at the beginning.

With the assumptions of incompressible fluid and zero energy loss, the relation between the pneumatic power exploited by Wells turbine and water elevation inside the chamber can be expressed as follows:

$$P_{pneumatic} = \Delta P. Q = C. Q^2 = C. S^2. \dot{h}^2 \qquad (19)$$

The generated pneumatic power is directly related to the OWC chamber surface S, the damping coefficient of Wells turbine C, and the vertical velocity of the piston inside the chamber $\dot{h}$ which is directly affected by ω_0 and γ [42]
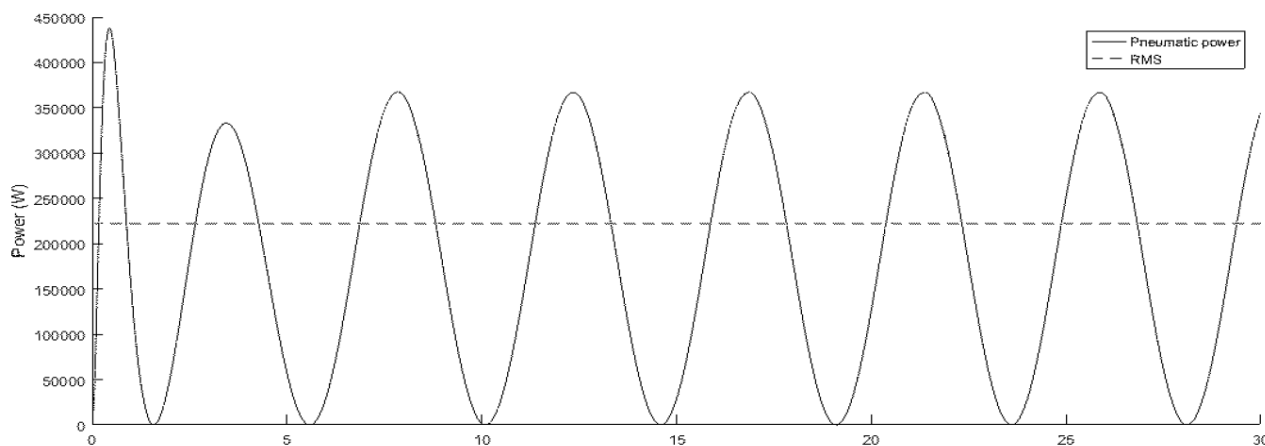
Figure 20: The OWC pneumatic power variation

As depicted in Figure 20, the power RMS value is designed with the dashed line indicating a power around 226kW. The optimal output turbine power value mentioned by F. R. Torres is 39.4 kW; for the model used, we neglected all sorts of energy losses (wall frictions, water viscosity, air viscosity…) [44]. For an efficiency of 17.5%, the results obtained for the pneumatic power seems logical. For better efficiency, it is always recommended to operate in the resonance domain, this is established when the damping γ is small and the incoming waves frequency matches with the natural frequency of the chamber ($\Omega \approx \omega_0$) .

The expressions of the natural frequency and the global damping of the OWC device, as mentioned in a previous equation, are:

$$\begin{cases} \omega_0 = \sqrt{\dfrac{g}{d}} \\ \gamma = \dfrac{C\,S}{\rho_e\,d} \end{cases} \qquad (20)$$

The resonance conditions, if established, allow acquiring the maximum pneumatic power by having h at extreme values. From equation (19), the power can be expressed in the resonance domain as follows:

$$P_{pneumatic} = CS^2\dot{h}^2 = CS^2\Omega^2 h^2 \qquad (21)$$

For the studied geometry, it can be noticed that the natural frequency ω_0 can be controlled only by fixing d, which is physically limited by the available sea depth D_{epth}. This leads to consider another geometrical shape or assumptions such as for chambers with parabolic or inclined sidewalls that provide additional geometrical parameters to control the natural frequency ω_0 [45] [37] [46]

By examining the global damping γ, it depends on the depth d, the Wells turbine damping C, and the base area surface S. As mentioned before, the global damping coefficient must be as low as possible to exploit the resonance phenomenon according to Figure 22. From the damping equation in the system (20), this can be applied only by taking the product $C.S$ as low as possible since d has been already fixed to obtain $\Omega \approx \omega_0$ (first condition of the resonance). However, this may affect the pneumatic power captured according to equation (21); a compromise should be established to ensure that the pneumatic power reaches its maximum in a region close to the resonance domain.

4. The Second Order Oscillator and Mechanical Analogy:

By adopting an analogy with mechanical systems, the linear part of the OWC differential equation is similar to the second-order mechanical oscillator one. This oscillator is made up mainly of spring with stiffness k, a damper with damping b, and a mass m excited by a force F(t) presented in Figure 21; mass motion satisfies the following differential equation:

$$m\frac{d^2y}{dt^2} + b\frac{dy}{dt} + ky = F(t) \qquad (22)$$
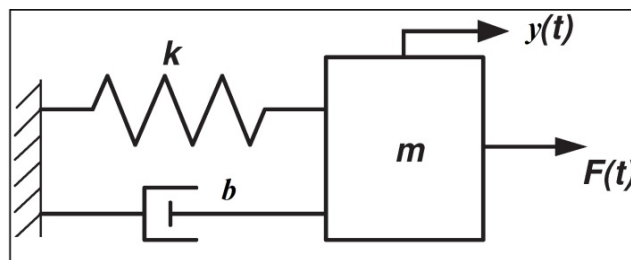
Figure 21: Simple mechanical oscillator

m, k, and b are the critical parameters of any mechanical oscillator. They determine the natural frequency and the damping given by [41]:

$$\omega_0^2 = {k}/{m} \quad ; \quad \gamma = {b}/{m} \qquad (23)$$

At a low elevation of h, the variation of water mass inside the chamber can be neglected, and the total mass M is approximately equal to $\rho_e S d$. Table 3 shows the parameters equivalence between the OWC system and mechanical oscillators.

Table 3: Analogy between the mechanical oscillator and the OWC system

	Mechanical oscillator	OWC (with low variation of h)	Unit
Mass	m	$M=\rho_e\,S\,d$	kg
Stiffness	k	$g\,\rho_e\,S$	N/m
Damping	b	$C\,S^2$	N.s/m

Studying the usual equation without considering the nonlinear term provides a good indication of the resonance regime, as shown in Figure 22, especially for low variation of h. This mechanical analogy helps to understand the behaviour of the water piston motion inside the OWC chamber.
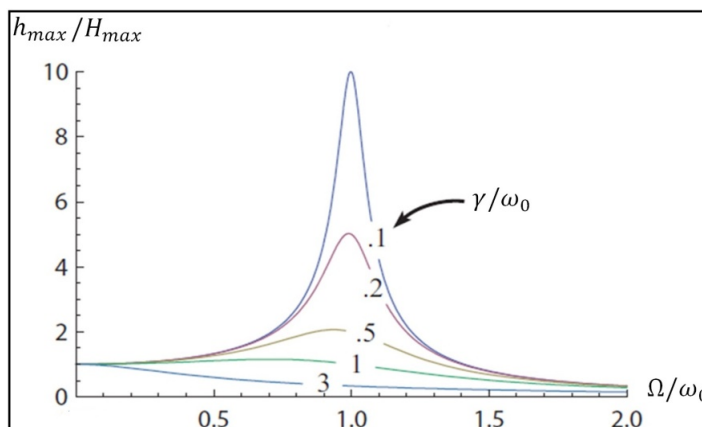
Figure 22: Dynamic system resonance

Thereafter, only the linear part of the wave differential equation is considered to establish an analogy with the Second-order oscillator systems and find an approached formulation.

We know that the expression of the differential equation of a second-order oscillator is:

$$\frac{d^2y(t)}{dt^2} + \frac{b}{m}\frac{dy(t)}{dt} + \frac{k}{m}y(t) = \frac{F(t)}{m} \qquad (24)$$

If an external force drives a damped oscillator, the motion equation solution has two parts: a transient and steady-state part. As we are interested only in the surface elevation inside the chamber after many periods, only the steady-state remains for the rest of our study, the expression in equation (25) describes the motion equation:

$$y_{steady}(t) = A\cos(\Omega t - \varphi) \qquad (25)$$

While: A is the displacement amplitude and φ is the angular dephasing [41]:

$$A = \frac{F/m}{\sqrt{(\Omega^2 - \omega_0^2)^2 + b^2\Omega^2/m^2}} \quad ; \quad \tan(\varphi) = \frac{b\Omega}{k - m\Omega^2} \qquad (26)$$

By applying the analogy of Table 3, water piston amplitude inside the chamber and the angular dephasing of its motion can be expressed as follows :

$$h_{max} = \frac{\omega_0^2\, H_{max}}{\sqrt{(\Omega^2 - \omega_0^2)^2 + \gamma^2\Omega^2}} \quad ; \quad \tan(\varphi) = \frac{\gamma\Omega}{\Omega^2 - \omega_0^2} \qquad (27)$$

Substituting the expressions with the numerical values for the F.R. Torres model leads to a maximum elevation of the piston inside the chamber h_{max} equal to $0.801m$ and an angular dephasing φ between the incident wave and the piston elevation equal to $0.76 rad$, which correspond to a time delay between the incident wave peak and the chamber wave elevation peak of $1.08 sec$. In conclusion: the numerical results of the simplified analogy expressions confirm graphs obtained in the simulation part.

The expression of piston elevation leads to deduce the expression of the airflow through the turbine, the pressure drop, and the pneumatic power in the case of the linear simplification assumption. The following equations (28), (29), and (30) show the expressions of these temporal variables:

$$q(t) = -S\Omega\, \frac{\omega_0^2 H_{max}}{\sqrt{(\omega_0^2 - \Omega^2)^2 + \gamma^2\Omega^2}}\, \sin(\Omega t + \phi) \qquad (28)$$

$$\Delta P(t) = -CS\Omega\frac{\omega_0^2\, H_{max}}{\sqrt{(\omega_0^2 - \Omega^2)^2 + \gamma^2\Omega^2}}\, \sin(\Omega t + \phi) \qquad (29)$$

$$P_{pneumatic}(t) = CS^2\Omega^2\, \frac{\omega_0^4\, H_{max}^2}{(\omega_0^2 - \Omega^2)^2 + \gamma^2\Omega^2}\cos^2(\Omega t + \phi) \qquad (30)$$

As for the RMS expression of the pneumatic power:

$$\overline{P_{pneumatic}} = \sqrt{\frac{3}{8}}CS^2\Omega^2\, \frac{\omega_0^4\, H_{max}^2}{(\omega_0^2 - \Omega^2)^2 + \gamma^2\Omega^2} \qquad (31)$$

The calculated value of the pneumatic power RMS that depends on F. R. Torres parameters choice is equal to $226kW$, which confirms graph results in Figure 20. In the resonance domain where $\Omega \approx \omega_0$ the theoretical output of the OWC device is maximal, and its RMS can be expressed as follows:

$$\overline{P_{resonance}} = \sqrt{\frac{3}{8}}CS^2\, \frac{\omega_0^4\, H_{max}^2}{\gamma^2}$$
$$= \sqrt{\frac{3}{8}\frac{(g\,H_{max}\rho_e)^2}{C}} \qquad (32)$$

The pneumatic power RMS value in the resonance domain for F. R. Torres chamber parameters is 503kW; this value is the maximal amount of energy that can be theoretically harvested by this air chamber coupled with the chosen turbine from an incident wave of 1m and a period of 9 sec.

In practical cases, the pneumatic power expression can be improved by adding a coefficient responsible for friction and viscosity energy loss μ [47]. This coefficient is always less than 1 and equal to 1 only when the viscosity and friction are neglected, as we did in the current model. Considering this condition, Equation (31) becomes:

$$\overline{P_{pneumatic}} = \sqrt{\frac{3}{8}\mu\frac{C(g\,H_{max})^2}{(\frac{d}{S\Omega})^2(\omega_0^2 - \Omega^2)^2 + (C/\rho_e)^2}} \qquad (33)$$

Equation (33) describes the essential components affecting the generated pneumatic power:

- The incident wave with its amplitude H_{max} and frequency Ω.
- The chamber design: especially the cross-section area S and the length of the submerged part d
- The choice of Wells turbine: the damping coefficient C.
- The quality of the process: energy loss via frictions and viscosity (coefficient μ)

It is interesting to see the influence of parameters that we can handle during the design: C for the Wells turbine choice, S and d for the chamber design. All OWC parameters are involved simultaneously; however, it is possible to fix two parameters and see the third one's influence to obtain a desired effective pneumatic power. The following equations (34), (35), and (36) reveal the expression of each parameter under these conditions.

$$S = d(\omega_0^2 - \Omega^2) / [\Omega\sqrt{\sqrt{\frac{3}{8}\mu\frac{C(g\,H_{max})^2}{P_{pneumatic}}} - (C/\rho_e)^2}] \qquad (34)$$

$$C = sol\{C^2 - [\sqrt{\frac{3}{8}\mu\frac{(\rho_e g\,H_{max})^2}{P_{pneumatic}}}]C + (\frac{d\rho_e}{\Omega S})^2(\omega_0^2 - \Omega^2)^2 = 0\} \qquad (35)$$

$$d = sol\{d^2 - \frac{2g}{\Omega^2}d + [(\frac{g}{\Omega^2})^2 + (CS/\Omega\rho_e)^2 - \sqrt{\frac{3}{8}\mu(\frac{S}{\Omega})^2\frac{C(g\,H_{max})^2}{P_{pneumatic}}}] = 0\} \qquad (36)$$

It is evident that the three equations do not always have a physical solution. There is some limitation on the pneumatic power that can be extracted.

For the chamber design and according to equations (34) and (36), regardless of the surface S and the length d choice, the pneumatic power cannot exceed a certain amount (the resonance condition):

$$\sqrt{\frac{3}{8}}\mu\frac{(\rho_e g\,H_{max})^2}{C} \geq \overline{P_{pneumatic}} \qquad (37)$$

Furthermore, with Wells turbine choice according to equation (35), the effective pneumatic power is also limited:

$$\sqrt{\frac{3}{8}}\mu\Omega S\rho_e\frac{(g\,H_{max})^2}{2d|\omega_0{}^2 - \Omega^2|} \geq \overline{P_{pneumatic}} \qquad (38)$$

It is possible to have a combination of the three parameters: surface and chamber depth in addition to the turbine damping to approach the resonance domain; however, there are other ways to improve the OWC generated pneumatic power like:

➢ Building the chamber in coastal structures such as breakwaters, seawalls, or jetties not only offers benefits in terms of construction costs but also improves wave height and energy concentration, especially in V structures [48].

➢ Searching regions with high waves amplitude is a priority; however, it is approved that area with regular waves can be more beneficial to the OWC performances [49] [50]

➢ The turbine choice is not limited by its damping; there are also some characteristics to consider during the design step (flow velocity, rotation speed, blade position…). Table 4 shows some used prototypes of the Wells turbine [51]:

Table 4: Wells turbine types used for wave energy conversion.

Wells turbine	Observations
Wells turbine with guide vanes [52]	It was adopted for the project "Mighty Whale" in Japan
Wells turbine with self-pitch-controlled blades	The turbine blades oscillate between two angles according to the flow direction, where the turbine has active pitch controlled blades
Biplane Wells turbine with guide vanes	This type is used in Islay, where the guide vanes are not necessarily adopted.
Contra-rotating Wells turbine	This turbine is installed in the LIMPET system in Islay, U.K. which is the world's first commercial wave power station

➢ Also, the design assumptions and the used methods to evaluate the OWC performances must not be neglected; in the current study, all hypotheses were simplified to construct solid arguments to see the implication of OWC parameters in its performances, Figure 23 sum up clearly all followed steps during this study. Still, there are many ways to improve this model, e.g., by considering an OWC with inclined sidewalls, variable cross-section or a multi-chamber OWC [45] [46] [53]. Nevertheless, this model can be regarded as a first tool to size and analyze an OWC device for better performance.
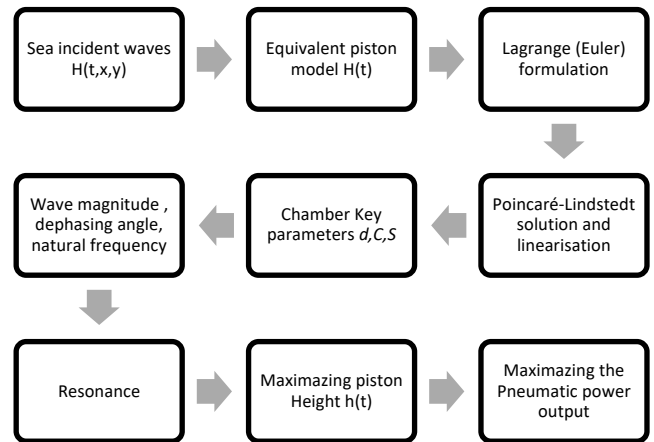
Figure 23: Proposed modelling steps to optimize the OWC performances

5. Conclusion:

In this paper, the studied OWC used for wave energy conversion was illustrated with a one-dimensional model based on water mass block moving upward and downward as a piston. The Lagrange formalism was applied to establish the governing differential equation. Analytical solutions of the first order were obtained successfully by applying the Poincaré–Lindstedt method. A parameter related to the chamber's submerged portion was then identified and used to solve the differential equation. The non-linearity effect on the dynamic behaviour of the considered system was examined. It was found that it has minor influences on the system operation. Then results were compared successfully with those obtained with Simulink software and by F. R. Torres simulation in the same conditions. As a conclusion, the elaborated model reveals similarities between the OWC device and any second-order mechanical oscillator, which are both characterized by their damping and natural frequency. Operating with an incoming wave frequency equal to the natural OWC frequency under low damping will theoretically amplify water elevation $h(t)$ inside the chamber. This case corresponds to the resonance condition. It was found that the natural frequency depends mainly on the depth of the submerged portion d, even though a combination of the chamber design parameters and the turbine choice must be carefully chosen in order to maximize the pneumatic power. This work is limited to the case of vertical OWC with a constant area and monochromatic sea waves driving the free water surface inside the chamber. However, its results and methodology may help to comprehend the essence of more complex models or even build powerful and efficient ones.

References

[1] T.M. Razykov, C.S. Ferekides, D. Morel, E. Stefanakos, H.S. Ullal, H.M. Upadhyaya,, "Solar photovoltaic electricity: current status and future prospects," Sol Energy, vol. 85, no. 8, p. 1580–608., 2011.

[2] N. Kannan , D. Vakeesan , "Solar energy for future world: A review," Renewable and Sustainable Energy Reviews , vol. 62, p. 1092–1105, 2016.

[3] A. Y. BATNIJI, R. MORJAN, M. S. ABDEL-LATIF, T. M. EL-AGEZ, S. A. TAYA, H. S. EL-GHAMRI, "Aldimine derivatives as photosensitizers for dye-sensitized solar cells," Turkish Journal of Physics, vol. 38, no. 1, p. 86–90, 2014.

[4] J. Gong, J. Liang, K. Sumathy, "Review on dye-sensitized solar cells (DSSCs):Fundamental concepts and novel materials", Renewable and Sustainable Energy Reviews, Volume 16, Issue 8, 2012, p 5848-5860

[5] H. S. El-Ghamri, T. M. El-Agez, S. A. Taya, M. S. Abdel-Latif and A. Y. Batniji, "Dye-sensitized solar cells with natural dyes extracted from plant seeds," Materials Science-Poland, vol. 32, no. 4, p. 547–554, 2014.

[6] Md T. Islam, Nazmul Huda, A.B. Abdullah, R. Saidur,, "A comprehensive review of state-of-the-art concentrating solar power (CSP) technologies: Current status and research trends," Renewable and Sustainable Energy Reviews, vol. 91, pp. 987-101, 2018.

[7] G.M. Joselin Herbert, S. Iniyan, E. Sreevalsan, S. Rajapandian,, "A review of wind energy technologies," Renewable and Sustainable Energy Reviews, vol. 11, no. 6, pp. 1117-1145, 2007.

[8] Ezio S, Claudio C., "Exploitation of wind as an energy source to meet the world's electricity demand.," Wind Eng, p. 74–76:375–87, 1998.

[9] Intergovernmental Panel on Climate Change., Special report on renewable energy sources and climate change mitigation : summary for policymakers and technical summary, 2012.

[10] A. F. O. Falcão, "Wave energy utilization: A review of the technologies", Renewable and Sustainable Energy Reviews, vol. 14, 2010, pp. 899-918.

[11] I. López, J. Andreu, S. Ceballos, I. Martínez De Alegría and I. Kortabarria, "Review of wave energy technologies and the necessary power-equipment", Renewable and Sustainable Energy Reviews, vol. 27, 2013, pp. 413-434.

[12] J. Bendfeld, S. Balluff and S. Krauter, "Green Energy from the Ocean An overview on costeffectiv and reliable measuring systems," International Conference on Renewable Energy Research and Applications (ICRERA), pp. 375-378, 2015.

[13] L. Rusu and F. Onea, "The performance of some state-of-the-art wave energy converters in locations with the worldwide highest wave power", Renewable and Sustainable Energy Reviews vol75, 2017, pp. 1348-1362.

[14] L. Duckers, Wave Energy, 2016, pp. 315-350.

[15] M. Takao and T. Setoguchi, "Air Turbines for Wave Energy Conversion," International Journal of Rotating Machinery, vol. 2012, pp. 1-10, 2012.

[16] K. Elatife and A. E. Marjani, "Optimized blade design of a radial impulse turbine for wave energy conversion," in Proceedings of 2015 IEEE International Renewable and Sustainable Energy Conference, IRSEC 2015, 2016.

[17] A. Palme, "Wave motion turbine," Power, , vol. 52, pp. 200-201, 1920.

[18] P. Ricci, "Modelling, Optimisation And Control Of Wave Energy Point-absorbers," thesis, University of LisbonLisbon, Portugal,, 2012.

[19] A. El Marjani, F. Castro Ruiz, M. A. Rodriguez and M. T. Parra Santos, "Numerical modelling in wave energy conversion systems," Energy, vol. 33, no. 8, pp. 1246-1253, 2008.

[20] A. Kamath, H. Bihs and Ø. A. Arntsen, "Numerical modeling of power take-off damping in an oscillating water column device," International Journal of Marine Energy, vol. 10, pp. 1-16, 2015.

[21] M. Horko, "CFD Optimisation of an Oscillating Water Column Wave Energy Converter," Thesis, The University of Western Australia, 2007.

[22] Y. K. a. K. K. T. Setoguchi, M. Takao, "Study on an Impulse Turbine for Wave Energy Conversion," International Society of Offshore and Polar Engineers, vol. 10, pp. 145-152, 2000.

[23] D. V. Evans and R. Porter, "Hydrodynamic characteristics of an oscillating water column device," Applied Ocean Research, vol. 17, no. 3, pp. 155-164, 1995.

[24] H. Bouhrim and A. El Marjani, "On the flow simulation based on piston models in OWC devices for wave energy conversion," in Proceedings of 2016 International Renewable and Sustainable Energy Conference, IRSEC 2016, 2017.

[25] R. M. D. Correia, "Modelação numérica da interação de ondas com uma estrutura de aproveitamento de energia das ondas do tipo coluna de agua oscilante," 2015.

[26] M. Takao, Y. Fujioka and T. Setoguchi, "Effect of pitch-controlled guide vanes on the performance of a radial turbine for wave energy conversion," Ocean Engineering, vol. 32, no. 17-18, pp. 2079-2087, 2005.

[27] T. H. Kim, T. Setoguchi, K. Kaneko and M. Takao, "The Optimization of Blade Pitch Settings of an Air Turbine Using Self-Pitch-Controlled Blades For Wave Power Conversion," Journal of Solar Energy Engineering, vol. 123, no. 4, p. 382, 2002.

[28] S. Wanan; L. Anthony, "Wave energy conversion of oscillating water column devices including air compressibility," Journal of Renewable and Sustainable Energy, vol. 8, no. 054501, 2016.

[29] D. Magagna, "Oscillating Water Column Wave Pump: A

Wave Energy Converter for Water Delivery," Thesis, University of Southampton, 2011.

[30] Z. J. You, "A close approximation of wave dispersion relation for direct calculation of wavelength in any coastal water depth," Applied Ocean Research, vol. 30, no. 2, pp. 113-119, 2008.

[31] A.F. Falcão, J.N.A. Sarmento, L. M.C. Gato, A. Brito-Melo, "The Pico OWC wave power plant: Its lifetime from conception to closure 1986–2018", Applied Ocean Research, Volume 98, May 2020, 102104

[32] A. F. Falcão and J. C. Henriques, "Oscillating-water-column wave energy converters and air turbines: A review", Renewable Energy, vol. 85, Elsevier Ltd, 2016, pp. 1391-1424.

[33] M. Takao, K. Yamada, M. M. Ashraful Alam, S. Okuhara, Y. Kinoue and S. Nagata, "Counter-rotating impulse turbine for wave energy conversion Performance improvement by means of middle van," IEEE 6th International Conference on Renewable Energy Research and Applications (ICRERA), pp. 111-114, 2017.

[34] W. Sheng, T. Lewis and R. Alcorn, "On wave energy extraction of oscillating water column device," in 4th International Conference on Ocean Energy, Dublin, 2012.

[35] R. Fitzpatrick (2018). Oscillations and Waves: An Introduction, Second Edition (2nd ed.). CRC Press. https://doi.org/10.1201/9781351063104

[36] A. El Barakaz and A. El Marjani, "The oscillatory free water surface motion inside OWC chamber for wave energy conversion," in Proceedings of 2016 International Renewable and Sustainable Energy Conference, IRSEC 2016, 2017.

[37] B. Kooverji, "Pneumatic Power Measurement of an Oscillating Water Column Converter," 2014.

[38] W. Sheng, R. Alcorn and A. Lewis, "Assessment of primary energy conversions of oscillating water columns. I. Hydrodynamic analysis," Journal of Renewable and Sustainable Energy, vol. 6, no. 5, 2014.

[39] Shuhui Ch'en, "Generalization of the Lindstedt-Poincaré method for analysis of non-linear vibrations," thesis, 1990.

[40] S. John Ashlin, S. A. Sannasiraj and V. Sundar, "Wave forces on an Oscillating Water Column device," Procedia Engineering, Vol 116, 2015, p 1019-1026,.

[41] D. Morin, Waves: Chapter 1 Oscillations, 2011.

[42] P. Filianoti and S. M. Camporeale, "A linearized model for estimating the performance of submerged resonant wave energy converters," Renewable Energy, vol. 33, no. 4, pp. 631-641, 2008.

[43] F. R. Torres, P. R. Teixeira and E. Didier, "Study of the turbine power output of an oscillating water column device by using a hydrodynamic–Aerodynamic coupled model," Ocean Engineering, vol. 125, pp. 147-154, 2016.

[44] A. F. O. Falcão, J. C. C. Henriques, L. M. C. Gato and R. P. F. Gomes, "Air turbine choice and optimization for

floating oscillating-water-column wave energy converter," Ocean Engineering, vol. 75, pp. 148-156, 2014.

[45] M. Iino, T. Miyazaki, H. Segawa and M. Iida, "Effect of inclination on oscillation characteristics of an oscillating water column wave energy converter," Ocean Engineering, vol. 116, pp. 226-235, 2016.

[46] M. J. Smith, J. J. Kobine and F. A. Davidson, "Free and forced motion in an asymmetric liquid-column oscillator," Proceedings of the Royal Society A: Mathematical, Physical and Engineering Sciences, vol. 464, no. 2092, pp. 905-922, 2008.

[47] R. q. Wang, D. z. Ning, C. w. Zhang, Q. p. Zou and Z. Liu, "Nonlinear and viscous effects on the hydrodynamic performance of a fixed OWC wave energy converter," Coastal Engineering, vol. 131, pp. 42-50, 2018.

[48] S. Zheng, Y. Zhang and G. Iglesias, "Coast/breakwater-integrated OWC: A theoretical model," Marine Structures, vol. 66, pp. 121-135, 2019.

[49] M. Li, R.-k. Wu, B.-j. Wu and Y.-q. Zhang, "Experimental Study on Conversion Efficiency of A Floating OWC Pentagonal Backward Bent Duct Buoy Wave Energy Converter," China Ocean Engineering, vol. 33, no. 3, pp. 297-308, 2019.

[50] M. Sanada, Y. Inoue and S. Morimoto, "Generator design and characteristics in direct-link wave power generating system considering appearance probability of waves," International Conference on Renewable Energy Research and Applications (ICRERA), pp. 1-6, 2012.

[51] A. S. Shehata, Q. Xiao, K. M. Saqr and D. Alexander, "Wells turbine for wave energy conversion: a review", International Journal of Energy Research vol. 41 , 2017, pp. 6-38.

[52] M. A. Alam, M. Takao, A. Takami, S. Okuhara, Y. Kinoue and T. Setoguchi, "Wells turbine with booster — Effect of guide vanes on the performance," IEEE International Conference on Renewable Energy Research and Applications (ICRERA), pp. 189-192, 2016.

[53] M. Shalby, P. Walker and D. G. Dorrell, "The investigation of a segment multi-chamber oscillating water column in physical scale model," IEEE International Conference on Renewable Energy Research and Applications (ICRERA), pp. 183-188, 2016.

APPENDICES

Appendix A: Lagrangian Formulation

The Lagrangian L^* consists of evaluating the difference between the kinetic energy T^* and the potential energy V^* of a system:

$$L^* = T^* - V^* \qquad (A.1)$$

The definition of Lagrange's equation:

$$\frac{d}{dt}\left(\frac{\partial T^*}{\partial \dot{h}}\right) - \frac{d}{dt}\left(\frac{\partial V^*}{\partial \dot{h}}\right) - \frac{\partial T^*}{\partial h} + \frac{\partial V^*}{\partial h} = F_{NC} \qquad (A.2)$$

Where: F_{NC} is the sum of all non-conservative forces.

The expression of the kinetic energy:

$$T^* = \frac{1}{2}\int v_{piston}{}^2 \, dM = \frac{1}{2}\rho_e S(h+d)\dot{h}^2 \qquad (A.3)$$

For terms in which the kinetic energy is involved:

$$\frac{d}{dt}\left(\frac{\partial T^*}{\partial \dot{h}}\right) = \rho_e S(\dot{h}^2 + (h+d)\ddot{h}) \qquad (A.4)$$

And:

$$\frac{\partial T^*}{\partial h} = \frac{1}{2}\rho_e S\dot{h}^2 \qquad (A.5)$$

We know that the potential of conservative forces does not depend on velocity:

$$\frac{d}{dt}\left(\frac{\partial V^*}{\partial \dot{h}}\right) = 0 \qquad (A.6)$$

To simplify, we can integrate the potential energy into the expression of total applied forces, using the following relation:

$$-\frac{\partial V^*}{\partial h} + F_{NC} = \sum F = F_2 - F_1 - g.M(t) \qquad (A.7)$$

By substituting equations (A.4), (A.5), (A.6), and (A.7) in equation (A.2), we obtain a differential equation for the piston motion:

$$\ddot{h} + \frac{C.S}{\rho_e.d}\dot{h} + \frac{g}{d}h + \frac{1}{d}\left[h\ddot{h} + \frac{1}{2}\dot{h}^2\right] = \frac{g}{d}H(t) \qquad (A.8)$$

Appendix B: Euler Formulation

In order to apply Euler formulation, a U tube model with different section S_1 and S_2 where the water level oscillates as described in Figure 24 which is a simplification of the OWC chamber model considered previously in Figure 4:   Geometry and characteristics of the chamber Figure 4
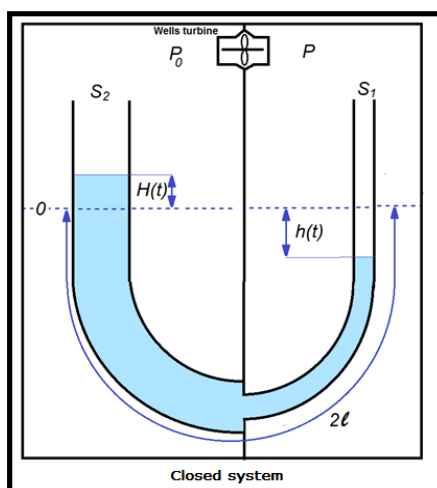
Figure 24: the OWC U tube model

From the definition of Euler equation (equation of the momentum):

$$\frac{D(\rho\vec{v})}{Dt} = -\overrightarrow{grad}P + \rho\vec{g} \qquad (B.1)$$

While: v is the flow velocity

With some simplifications, we obtain:

$$\rho\left(\left(\frac{\partial \vec{v}}{\partial t}\right) + \overrightarrow{grad}\left(\frac{v^2}{2}\right) - \vec{v}\wedge\overrightarrow{rot}\vec{v}\right)$$
$$= -\overrightarrow{grad}P + \rho\vec{g} \qquad (B.2)$$

$$\frac{\partial \vec{v}}{\partial t} + \overrightarrow{grad}\left(\frac{v^2}{2}\right) - \vec{v}\wedge\overrightarrow{rot}\vec{v}$$
$$= -\frac{\overrightarrow{grad}P}{\rho} + \overrightarrow{grad}(-gz) \qquad (B.3)$$

$$\frac{\partial \vec{v}}{\partial t} + \overrightarrow{grad}\left(\frac{v^2}{2} + \frac{P}{\rho} + g.z\right) - \vec{v}\wedge\overrightarrow{rot}\vec{v} = 0 \qquad (B.4)$$

After a scalar multiplication by the element $\overrightarrow{dl}$ parallel to the streamlines:

$$\frac{\partial \vec{v}}{\partial t}.\overrightarrow{dl} + \overrightarrow{grad}\left(\frac{v^2}{2} + \frac{P}{\rho} + g.z\right)\overrightarrow{dz} - \vec{v}\wedge\overrightarrow{rot}\vec{v}.\overrightarrow{dz} = 0 \qquad (B.5)$$

Hence:

$$\frac{\partial \vec{v}}{\partial t}.\overrightarrow{dl} + d\left(\frac{v^2}{2} + \frac{P}{\rho} + gz\right) = 0 \qquad (B.6)$$

Then integration between h and H elevations:

$$\int_h^H \frac{\partial \vec{v}}{\partial t}.\overrightarrow{dl} + \left[\frac{v^2}{2} + \frac{P}{\rho} + gz\right]_h^H = 0 \qquad (B.7)$$

As water is incompressible, its velocity v depends only on the section; the flow remains the same:

$$Q = S.v = S_1.v_1 = S_2.v_2 \qquad (B.8)$$

So the velocity has two value depending on the cross-section:

$$v = \begin{cases} h > x > -l : \ v_1 = \dot{h} \\ -l > x > -2l + H : \ v_2 = \dfrac{S_1}{S_2}\dot{h} \end{cases} \qquad (B.9)$$

Then from the equation (B.7):

$$\int_h^{-l} \ddot{h}\,\overrightarrow{dl} + \int_{-l}^{-2l-H} \frac{S_1}{S_2}\ddot{h}\,\overrightarrow{dl} + \left[\frac{v^2}{2} + \frac{P}{\rho} + g.z\right]_h^H = 0 \qquad (B.10)$$

$$\ddot{h}\left(\left(\frac{S_1}{S_2} + 1\right)l + \frac{S_1}{S_2}H + h\right) + \frac{\dot{h}^2}{2}\left(1 - \left(\frac{S_1}{S_2}\right)^2\right)$$
$$+ \frac{P - P_0}{\rho} + g(h - H) = 0 \qquad (B.11)$$

By replacing S_1 and S_2 with chamber and sea surface and l with the depth of chamber d, the ratio S_1/S_2 is neglected, and the final equation is the same as the one obtained in the Lagrangian formulation:

$$\ddot{h}(d + h) + \frac{\dot{h}^2}{2} + \frac{P - P_0}{\rho} + g(h - H) = 0 \qquad (B.12)$$

Finally:

$$\ddot{h} + \frac{C.S}{\rho_e.d}\dot{h} + \frac{g}{d}h + \frac{1}{d}[h\ddot{h} + \frac{1}{2}\dot{h}^2] = \frac{g}{d}H(t) \qquad (B.13)$$

Appendix C: Poincaré–Lindstedt Method

The initial conditions are:

$$\begin{cases} h(0) = h_{max} \\ \dot{h}(0) = 0 \end{cases} \qquad (C.14)$$

We define $\epsilon = 1/d$ and equation (12) becomes:

$$\ddot{h} + \omega_0^2 h + \epsilon\left[h\ddot{h} + \frac{1}{2}\dot{h}^2\right] = 0 \qquad (C.15)$$

As long as ϵ is a small parameter comparing to h_{max}, the method of Poincaré–Lindstedt first-order becomes more accurate, otherwise higher orders are suggested.

To apply Poincaré–Lindstedt (first-order), we need to consider new variables:

$$\begin{cases} \omega = \omega_0 + \epsilon\omega_1 \\ \varphi = \omega t \\ x(\varphi) = h(t) \\ x(\varphi) = x_0(\varphi) + \epsilon x_1(\varphi) \end{cases} \qquad (C.16)$$

Then:

$$\begin{cases} h(t) = x(\varphi) \\ \dot{h}(t) = \omega\frac{dx}{d\varphi} = \omega x'(\varphi) \\ \ddot{h}(t) = \omega^2\frac{d^2x}{d\varphi^2} = \omega^2 x''(\varphi) \end{cases} \qquad (C.17)$$

After substituting the old variables with the new ones:

$$\omega^2 x'' + \omega_0^2 x + \epsilon\left(\omega^2 x'' x + \frac{1}{2}\omega^2 x'^2\right) = 0 \qquad (C.18)$$

Then:

$$\begin{aligned} (\omega_0 + \epsilon\omega_1)^2(x''_0 + \epsilon x''_1) + \omega_0^2(x_0 + \epsilon x_1) + \epsilon(\omega_0 \\ + \epsilon\omega_1)^2[(x''_0 + \epsilon x''_1)(x_0 + \epsilon x_1) \\ + \frac{1}{2}(x'_0 + \epsilon x'_1)^2] = 0 \end{aligned} \qquad (C.19)$$

After that, we ignore the terms with coefficients of order greater than ϵ^1:

$$\begin{aligned} (\omega_0^2 x''_0 + \epsilon\omega_0^2 x''_1 + 2\epsilon\omega_0\omega_1 x''_0) + (\omega_0^2 x_0 \\ + \epsilon\omega_0^2 x_1) \\ + \left(\epsilon\omega_0^2 x''_0 x_0 + \frac{1}{2}\epsilon\omega_0^2 x'^2_0\right) = 0 \end{aligned} \qquad (C.20)$$

$$\begin{aligned} \omega_0^2 x''_0 + \omega_0^2.x_0 + \epsilon(2\omega_0\omega_1 x''_0 + \omega_0^2 x''_1 + \omega_0^2 x_1 \\ + \omega_0^2 x''_0 x_0 + \frac{1}{2}\omega_0^2 x'^2_0) = 0 \end{aligned} \qquad (C.21)$$

By isolating each order of ϵ, the result is a system of two differential equations:

$$\epsilon^0: \quad x''_0 + x_0 = 0$$

$$\epsilon^1: \quad x''_1 + x_1 = -\frac{x'^2_0}{2} - x''_0 x_0 - 2\left(\frac{\omega_1}{\omega_0}\right)x''_0 \qquad (C.22)$$

Initial conditions:

$$\begin{cases} x_0(0) = h_{max} \\ x'_0(0) = 0 \end{cases} \quad \begin{cases} x_1(0) = 0 \\ x_1'(0) = 0 \end{cases} \qquad (C.23)$$

The solution for $x_0(\varphi)$ can be easily written:

$$x_0(\varphi) = h_{max}\cos(\varphi) \qquad (C.24)$$

Then we substitute $x_0(\varphi)$ in the second equation of the system, to solve $x_1(\varphi)$:

$$\begin{aligned} x_1(\varphi) = -h_{max}.(\omega_1/\omega_0)\cos(\varphi) \\ - \frac{1}{2}h_{max}[-2.(\omega_1/\omega_0)\varphi\sin(\varphi) \\ + h_{max}\cos^2(\varphi) \\ - 2(\omega_1/\omega_0)\cos(\varphi) - h_{max}] \end{aligned} \qquad (C.25)$$

The coefficient ω_1 must equal to zero. Otherwise, the solution includes a divergent term (the secular term $2\frac{\omega_1}{\omega_0}\varphi\sin(\varphi)$).

Thus, once the divergence problem is eliminated, $x_1(\varphi)$ can be expressed as follows:

$$x_1(\varphi) = h_{max}^2(1 - \cos^2(\varphi))/2 \qquad (C.26)$$

Finally, the solution $h(t)$ can be written as:

$$h(t) = x_0(\omega t) + \epsilon x_1(\omega t) \qquad (C.27)$$

$$h(t) = h_{max}\cos(\omega_0 t) + h_{max}^2(1 - \cos^2(\omega_0 t))/2d \qquad (C.28)$$